Journal of Radioanalytical and Nuclear Chemistry (2023) 332:4179–4190
https://doi.org/10.1007/s10967-023-09100-2

Effective adsorption of U(VI) onto phosphate- and amine-linker-based organic polymer

Yaoxuan Wang[1,2,3] · Siyihan Duan[1,2,3] · Wanrong Song[1,2,3] · Tao Duan[1,2,3] · Lin Zhu[1,2,3]

Received: 19 May 2023 / Accepted: 2 August 2023 / Published online: 24 August 2023
© Akadémiai Kiadó, Budapest, Hungary 2023

Abstract

The efficient removal of uranium from aqueous solutions is critical for ecological safety. Herein, a novel phytic acid and melamine covalent polymer adsorbent (named PEM) was designed and synthesized through a simple one-pot method, and its adsorption performance and mechanism of U(VI) were systematically investigated. The maximum adsorption capacity on U(VI) achieved 505.05 mg g^{-1} at pH 4.0, calculated with the Langmuir model, which was much higher than most other adsorbents under the same environment. Importantly, the reaction reached equilibrium quickly in the initial 20 min at 298 K. The sorption process conformed to a pseudo-second-order kinetics model and Langmuir model, indicating that the chemisorption of the monolayer was dominant. Overall, the synthesized PEM could be utilized as an easy, efficient, less time-consuming material for the removal of uranium from acidic nuclear wastewater.

Graphical abstract

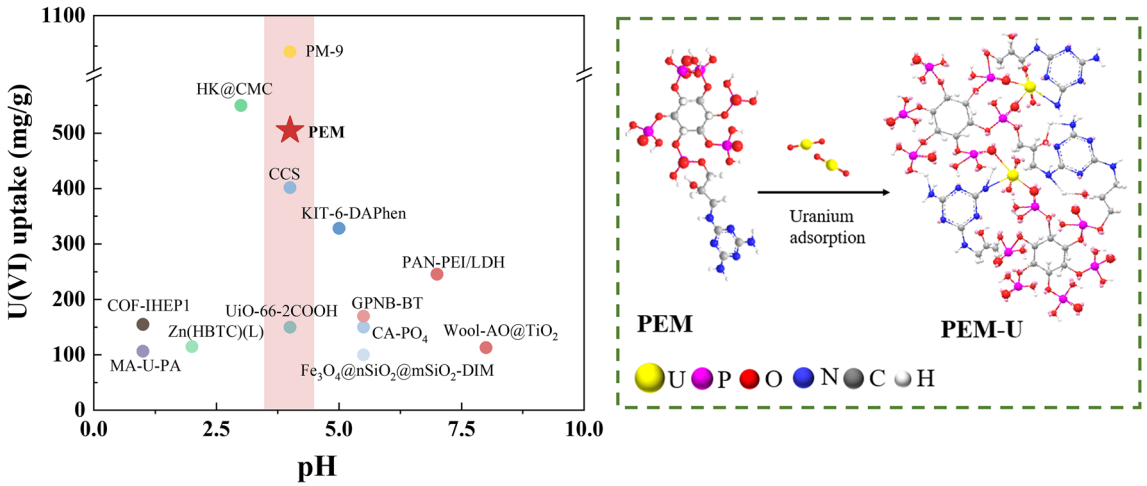

Keywords Uranium adsorption · Phosphate groups · Amine groups · Nuclear wastewater · Covalent polymer

Yaoxuan Wang, Siyihan Duan and Wanrong Song have contributed equally to this work.

✉ Tao Duan
duant@ustc.edu.cn

✉ Lin Zhu
zhulin@swust.edu.cn

[1] State Key Laboratory of Environment-Friendly Energy Materials, Southwest University of Science and Technology, Mianyang 621010, China

[2] Tianfu Institute of Research and Innovation, Southwest University of Science and Technology, Chengdu 610299, China

[3] National Co-Innovation Center for Nuclear Waste Disposal and Environmental Safety, Southwest University of Science and Technology, Mianyang 621010, China

Introduction

With the rapid development of science, technology, and the economy, the demand for energy resources has been surging. Today, the increasing consumption of nonrenewable resources, such as oil, coal, and natural gas, renders a shortage of energy as well as the massive emission of hazardous gases [1]. It is thus extremely urgent to search for environmentally respectful, sustainable, and renewable energy alternatives to fossil fuels. With a low-carbon footprint, nuclear energy plays a significant role in the global energy system. Among all the nuclear fuels, Uranium is the most important and crucial resource for nuclear power [2, 3]. However, a large part of the radioactive waste is produced by uranium mining, smelting, and spent fuel reprocessing, which have different levels of radioactivity [4]. That may become a severe hazard for humankind and exhibit long-lasting consequences for the environment [5]. It is upon this background that finding efficient techniques to treat uranium-containing radioactive water has become a global issue.

To date, several approaches have been applied for effective purification of uranium-containing radioactive water, including chemical precipitation [6], membrane filtration [7], concentration by rotary evaporation [8], ion exchange [9], adsorption [10], solid phase extraction [11], biosorption processes [12], and so on. Of these, adsorption has been widely used in the treatment of uranium in wastewater due to its simplicity, convenience, fast kinetics, cost-saving, and non-secondary contamination [10]. In the past few decades, lots of adsorbents have been explored, such as metal–organic frameworks (MOFs) [13], metal oxides materials, mineral materials, carbon-based materials, inorganic materials, chelating resins, porous organic frameworks (POFs), clay minerals, polymeric materials [14–18]. The inorganic and carbon-based materials usually show a low adsorption capacity and limited selectivity for uranium, while the metal–organic frameworks (MOFs) are confined to their high cost for synthesis and difficult recyclability [19, 20]. Polymeric materials have been widely studied as efficient adsorbents for uranium due to their highly accessible and cost-effective raw materials, moreover, they can be modified with suitable functional groups so as to attain diverse properties including vast surface area, and excellent mechanical rigidity [21]. Some high-affinity ligands, such as oxime, amidoxime, imidazole, carboxyl or phenolic, amine, and phosphonate groups, make polymeric adsorbents more promising. Among them, amidoxime has been paid much attention to in recent years because it can not only form strong interaction between amidoxime ligands and U(VI) but have high selectivity towards U(VI). Xing Zhong et al. prepared a crosslinked amidoxime-functionalized β-cyclodextrin polymer (β-CDP-AO) by introducing amidoxime groups on β-Cyclodextrin polymer (β-CDP). The experimental result showed that the material could reach equilibrium in 2 h and the maximum adsorption amount for U(VI) was 221.54 mg g^{-1} at pH = 6.0 after modification. In addition, a recent overview presented by Tang et al. in terms of amidoxime-based materials for uranium treatment offered guidance and advice for the design of novel amidoxime-based materials [22]. Phosphate moieties have a strong affinity with highly valent radionuclides because of the good coordinating ability of O-donating phosphate ligands. Compare to amidoxime, phosphonate has a better adsorption ability under more acidic conditions. Previous studies have pointed out that tri-butyl-phosphate (TBP) and trioctyl-phosphine oxide (TOPO) showed great interactions with U(VI) [23]. To circumvent the problem of uranium adsorption under highly acidic conditions, Yu et al. designed phosphonate-decorated covalent organic frameworks named COF-IHEP1 and COF-IHEP2. The combination of phosphonate and COFs endowed materials with a record adsorption capacity of 112 mg g^{-1} in 1 M HNO_3 solution [24, 25]. Budnyak et al. reported a new imidazole-2yl-phosphonic acid/mesoporous silica sorbent ($ImP(O)(OH)_2/SiO_2$), which was applied in uranium removal with the highest adsorption capacity exceeding 618 mg g^{-1} at pH 4 [26]. Jayakumar et al. gave a short but informative review, which could be a reference for the preparation of phosphorylated adsorbents [27].

Melamine (MA) contains three amino groups and three aromatic nitrogen atoms, which have great potential for the adsorption of heavy metals [28]. Wang et al. synthesized melamine-modified graphene hydrogels (MA-GH) with a three-dimensional network structure by one-step hydrothermal method. The introduction of the nitrogen-containing functional groups conferred good uranium adsorption properties to MA-GH, in which the optimal uranium adsorption capacity could reach 186.27 mg g^{-1} [29]. Phytic acid (PA) ($C_6H_{18}O_{24}P_6$) is a natural, nontoxic compound with six phosphate groups, and its phosphate sites can chelate with metal ions via a strong covalent bond [30]. Therefore, PA is used as a surface functionalization group to modify the substrate material. Pan et al. chose the materials containing phosphoric acid using PA and MA as the two organic building blocks as an adsorbent for the fast adsorption and recovery of uranium from acidic aqueous media, and it possessed fast adsorption kinetic, high adsorption capacity up to 1034.9 mg g^{-1} and excellent selectivity [31].

In this study, a simple method was applied to first prepare PA and MA covalent polymer (PEM) adsorbent. The materials were characterized in detail with XRD, SEM, FT-IR, Raman, BET, and XPS. Afterward, the removal of U(VI) by PEM was studied by performing batch experiments under

a series of environmental conditions such as pH, temperature, and concentration of U(VI). In addition, the possible structure of PEM and underlying removal mechanisms were further speculated on the basis of the experimental results.

Experimental

Chemicals and reagents

All chemicals (analytical grade) were used as received without any further purification. Deionized water was used for all experiments. $UO_2(NO_3)_2{\cdot}6H_2O$ (≥ 99.9% purity) was purchased from the Beijing chemical factory. The potassium carbonate was purchased from Tianjin Kemiou Chemical Reagent Co. Ltd., China. All other chemicals, including PA solution ($C_6H_{18}O_{24}P_6$, 70% in H_2O), MA ($C_3H_6N_6$, 99%), epichlorohydrin (C_3H_5ClO), and *N*,*N*-dimethylformamide (DMF, C_3H_7NO, 99.5%) were purchased from Aladdin Reagent (Shanghai) Co., Ltd.

Synthesis of PEM

First, 4.72 g of PA was weighed into the Teflon liner of the autoclave with an electronic balance, then 1.26 g of MA was added, and 60 mL of DMF was poured into the Teflon liner. The mixture was then stirred continuously at 30 °C. During stirring, 20 mL of epichlorohydrin was slowly added dropwise, and then 1.0 g of potassium carbonate was added. After stirring, the sealed Teflon-lined autoclave was put into a 65 °C oven for 6 h. 6 h later, the oven was heated to 100 °C for 8 h. After cooling down, the block-like product was poured into a beaker and broken up with a glass rod, then separated by suction filtration, and the filtrate was extracted twice with deionized water. After that, the separated product was placed into centrifuge tubes containing absolute ethanol and centrifuged three times for 5 min each. The supernatant was removed, and the precipitate was dried in an oven at 60 °C.

Batch adsorption experiments

Batch adsorption experiments were conducted to explore the adsorption behavior of U(VI) on the PEM sorbent in the aqueous solution and investigate the influence of factors including pH, temperature, initial U(VI) concentration, and contact time on uranium adsorption. These experiments were conducted in a water bath shaker at 150 rpm min^{-1} and in constant temperature conditions. Then, the mixture solution was filtered by a nylon membrane with a pore size of 22 μm. The ultraviolet–visible spectrophotometer with a wavelength of 650 nm was carried out to measure the mass of the remaining uranium in the sample vials.

In addition, all the experiments contained two groups, which were established at the same temperature, pH, ionic strength, and initial uranium concentration. It included the experimental group (uranium solution and PEM polymer) and blank control group (uranium solution), which were set up to avoid the additional impact of uranyl hydrolysis and ensure the authenticity and accuracy of the experiment. The adsorption capacity and removal efficiency were calculated using the following equation:

$$q_t = \frac{(C_0 - C_e)}{m} \times V \quad (1)$$

$$R = \frac{C_0 - C_e}{C_0} \times 100\% \quad (2)$$

where q_t (mg g^{-1}) is the adsorption capacity of the adsorbent, R (%) is the removal efficiency, C_0 (mg L^{-1}) is the original concentration of uranium solution, and C_e (mg L^{-1}) is the concentration of uranium(VI) solution at equilibrium. V (L) and m (g) designate the volume of the solution and the weight of the sorbent, respectively.

Characterization

The morphologies of all materials were taken by scanning electron microscopy (SEM, Zeiss Ultra 55). The elements of the samples were analyzed by Energy Dispersive X-Ray Spectroscopy (EDX). The structures of materials were tested by Fourier transforms infrared spectroscopy (FT-IR), Raman, and X-ray diffraction (XRD). Specific areas were calculated by applying the BET method. The BET surface areas of PEM were recorded by a micrometric ASAP 2460 apparatus under 77 K. FT-IR spectra were observed on Fourier transforms infrared spectroscopy (FT-IR, Nicolet 5700) with the wavenumber ranging from 400 to 4000 cm^{-1}. Raman measurements were performed in a Renishaw system with a 514 nm laser. The XRD patterns were collected on a *D*/max 2500 with a Cu Ka source ($k = 1.541$ Å) at a scanning rate of 6°/min for 2 h, ranging from 5° to 70°. X-ray photoelectron spectroscopy (XPS) was conducted on a Thermal XPS ESCALAB 250Xi Spectrometer. All peaks were calibrated by setting the C1*s* peak of 284.6 eV as a reference.

Results and discussion

Characterization of the materials

As shown in Fig. 1, the XRD pattern exhibited 5 peaks at 17.65°, 21.62°, 26.17°, 28.78°, and 29.78°, which were in agreement with MA (JCPDS No. 24-1654). However, almost no MA peak could be identified for the synthesized PEM, and a broad and weak diffraction peak appeared, which indicated that the structure of MA was altered by

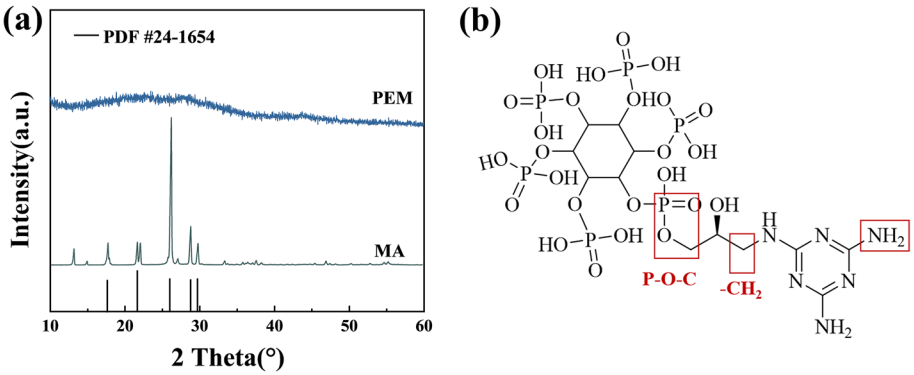

Fig. 1 **a** XRD pattern of MA and PEM. **b** Structure of PEM

the addition of PA and epichlorohydrin, and the synthesized PEM was amorphous.

In SEM characterization, Fig. 2, it could be seen that PEM has a rough, coral-like, and porous morphology. According to the EDS spectrum and element mapping image, the N and P elements were uniformly distributed on PEM, suggesting the successful combination of PA and MA.

FT-IR spectra and Raman spectra were measured to study the interactions of raw materials. In Fig. 3a, peaks at 3469.09, 3419.48, and 3129 cm^{-1} in MA were assigned to the stretching vibration of NH_2. By contrast, the NH_2 stretching vibration bands were weakened in the PEM, signifying the NH_2 groups participate in the synthesis. The characteristic adsorption peaks of epoxy groups in the range of 1280–1180 cm^{-1} and the –OH peak of PA in the range of 3700–2200 cm^{-1} disappeared as well as a $–CH_2$ adsorption peak at 2922.2 cm^{-1} appeared in PEM, which suggested the ring opening of epichlorohydrin and its involvement in the subsequent polymerization reaction [32]. Compared to the obvious signal of P–O–C at 1030 cm^{-1} in PEM, the PA showed almost no P–O–C adsorption peak. It was speculated that the electronegativity of the P–O–C group in PA increased after forming PEM, simultaneously, the epichlorohydrin reacted with PA creating a new P–O–C group [31, 33–35]. Additionally, the characteristic peaks of –Cl revealed in PEM at 531.1 cm^{-1} implied the no-thoroughly removal of –Cl. But the contents of by-products were relatively low, which could be seen from the EDS results in Fig. 2a–1. Raman spectra was presented in Fig. 3b. For MA, the peak at 1436 cm^{-1} was attributed to the C=N stretching vibration, while the peaks at both 1557 cm^{-1} and 3126 cm^{-1} were $–NH_2$ stretching vibrations. Whereas in PEM, the characteristic peaks of $–NH_2$ largely decreased or nearly disappeared, which supports the results of FT-IR that the reaction took place at the $–NH_2$. The Raman spectrum of PA in Fig. S1 was plotted in the range of 400–1500 cm^{-1}. By comparing the bands of the MA and the physical mixture of PA and MA (PA + MA), it could be found that the $–NH_2$ peak at 3126 cm^{-1} shifted to a lower frequency in

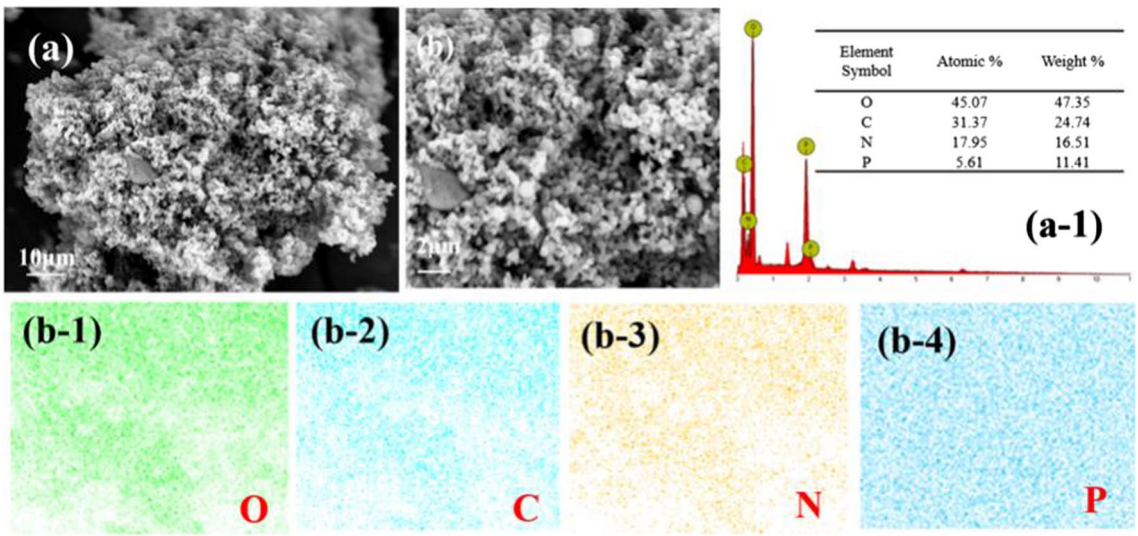

Fig. 2 SEM and EDS spectrum images of PEM

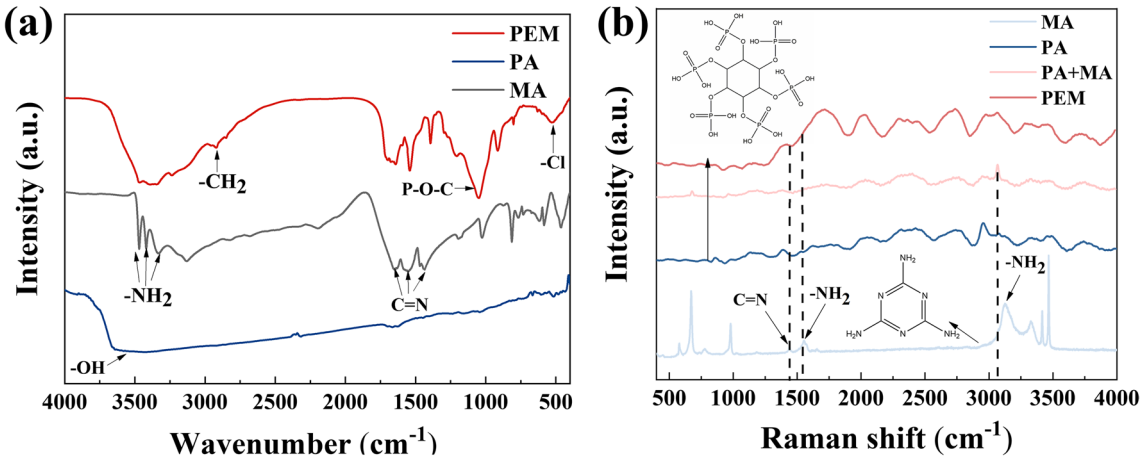

Fig. 3 **a** FT-IR spectra of PEM, PA, and MA. **b** Raman spectrum of MA, PA, MA + PA (the physical mixture of PA and MA), and PEM

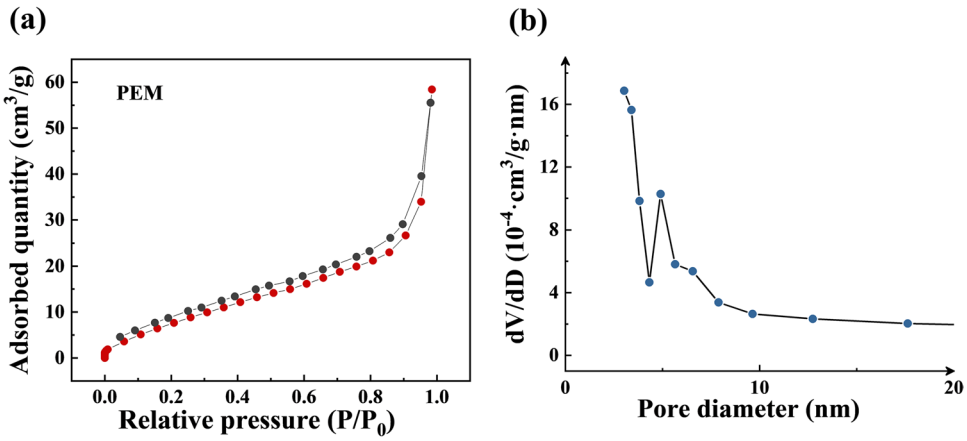

Fig. 4 **a** Nitrogen adsorption–desorption isotherm and **b** BJH pore size distribution of PEM measured at 77 K

PA + MA. This was probably the formation of the hydrogen bond of PA with MA. Furthermore, from PA + MA to PEM the Raman spectrum underwent a distinct change because the epichlorohydrin played a major role, which also agreed with the result of FT-IR.

The surface area and porous properties of PEM were studied by an N_2 adsorption–desorption measurement at 77 K in Fig. 4a. In the low-pressure region ($P/P_0 = 0$–0.001), the PEM showed significant N_2 absorption, indicating the existence of substantial micropores. In the medium-pressure range ($P/P_0 = 0.3$–0.8), the absorption curve kept growing, suggesting the presence of mesopores in this material. While in the high-pressure area, it exhibited an obvious upward trend, which indicated the containing of macropores. The BET surface area and the total pore volume were calculated in Table 1. Finally, the respective BJH pore size distribution curve was given in Fig. 4b, and the average pore diameter was 15.146 nm [36]. Collectively, the structure of the PEM was drawn in Fig. 1b.

Table 1 Porosity parameters of the PEM

Sample	BET surface area ($m^2\ g^{-1}$)	Total pore volume ($cm^3\ g^{-1}$)	Average pore diameter (nm)
PEM	30.523	0.09036	15.146

Adsorption experiments

Effect of pH

As shown in Fig. 5a, it was clear that the adsorption of U(VI) on PEM was pH dependent, and the optional pH value was 4.0. Error bars in Fig. 5a were shown the high accuracy of the experimental data. The variation trend could be ascribed to both the hydrogen ion concentration and uranium species.

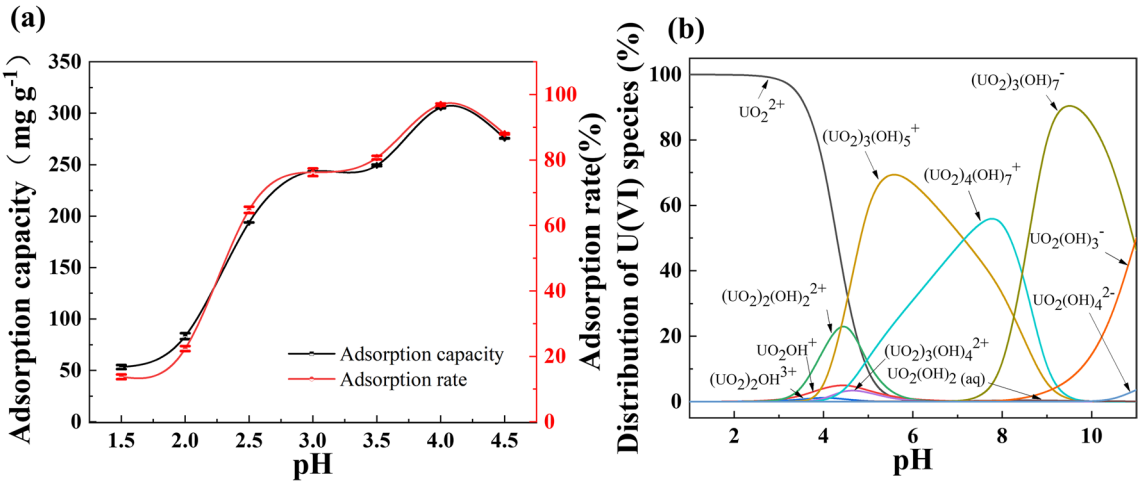

Fig. 5 **a** The effect of pH on adsorption of U(VI) (C_0 = 160 mg L^{-1}, $m_{sorbent}/V_{solution}$ = 0.5 mg mL^{-1}, T = 298 K, Time = 60 min). **b** The distribution of U(VI) in pH = 1.0–11.0

When the pH value was less than 2.0, UO_2^{2+} was the predominant form, and H^+ in the solution had a positive charge and competed with uranyl ions for active sites of the PEM, leading to a relatively low adsorption capacity. While the capacities enhanced with the rise of pH (pH value was less than 4.0) because of the decrease in the concentration of H^+. However, the capacities decreased with the increase of pH (pH value was higher than 4.0), which was due primarily to that the uranium exists mainly in the states of some stable polynuclear hydroxide complexes (such as UO_2OH^+, $(UO_2)_2(OH)_2^{2+}$, $(UO_2)_3(OH)_5^+$) with lower adsorption affinities and larger ionic radii than UO_2^{2+} [37–39]. Above all, the adsorption of UO_2^{2+} by PEM is mainly aimed at uranyl ions in a weak acid solution environment.

Adsorption kinetics

By changing the contact time from 0 to 120 min, the adsorption kinetics of the PEM was investigated at pH = 4.0 and 298 K. The results were listed in Fig. 6. The reaction speed was conspicuously fast in the initial 20 min and it reached equilibrium around 20 min at 298 K. Moreover, Fig. S2 demonstrated that the removal rate of PEM could achieve 99.08% through 40 min. To understand the sorption process mechanism of U(VI) onto PEM, the pseudo-first-order model and the pseudo-second-order model, which were expressed as the following formulas were used to fit the data:

$$\text{The pseudo - first - order equation: } \mathrm{Ln}\left(q_e - q_t\right) = \mathrm{Ln}q_e - K_1 t \quad (3)$$

$$\text{The pseudo - first - order equation: } \mathrm{Ln}\left(q_e - q_t\right) = \mathrm{Ln}q_e - K_1 t \quad (4)$$

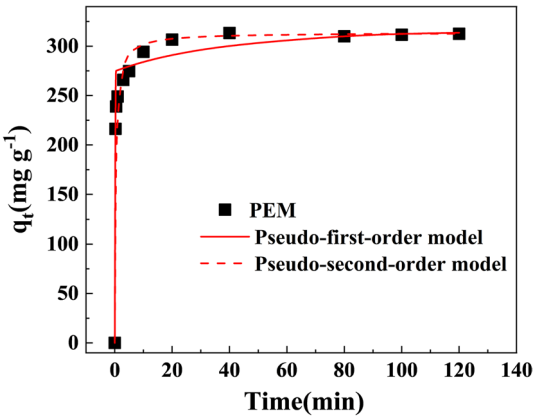

Fig. 6 The effect of time on the adsorption of U(VI) (C_0 = 160 mg L^{-1}, pH = 4.0, $m_{sorbent}/V_{solution}$ = 0.5 mg mL^{-1}, T = 298 K) and adsorption kinetic model of U(VI) adsorption for PEM

where the q_t and q_e correspond to the sorption amount (mg g^{-1}) at time t and the equilibrium sorption amount of kinetic models, respectively. k_1 (min^{-1}) and k_2 (mg g^{-1} min^{-1}) are denoted as the sorption rate constants.

The fitting plots as well as the parameters were given in Fig. S3 and Table S1. It well found that the correlation coefficient of the pseudo-second-order model (R^2 = 0.99994) was higher than the pseudo-first-order model (R^2 = 0.129). The equilibrium adsorption capacity calculated by pseudo-second-order was 312.5 mg g^{-1}, which was highly similar to the experimental value (315.2 mg g^{-1}). The above conclusion indicated that the adsorption behavior of U(VI) on PEM was chemical adsorption rather than physics adsorption.

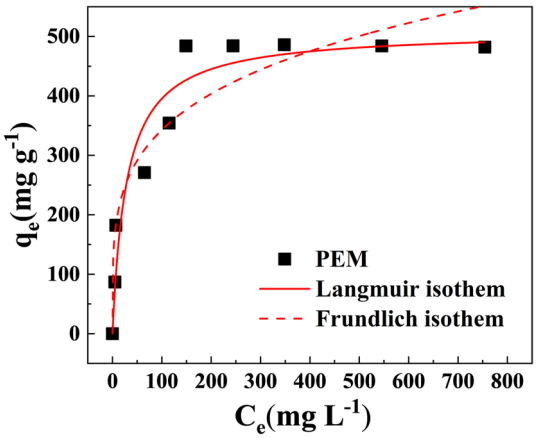

Fig. 7 The effect of C_0 on the adsorption of U(VI) (pH = 4.0, $m_{sorbent}/V_{solution}$ = 0.5 mg mL^{-1}, T = 298 K, Time = 60 min) and adsorption isotherm model of U(VI) adsorption for PEM

Adsorption isothermal

The initial concentration of the uranium also plays an important role during the adsorption process. Keeping the solid–liquid ratio constant, the adsorption isotherm of U(VI) by the PEM was determined by changing the initial U(VI) concentration (5–200 mg L^{-1}) at pH = 4.0 and 298 K. In Fig. 7, as the concentration of uranium increased, the adsorption capacity went up first and then stay constant, which was because the amount of uranium increased thereby leading to a stronger interaction between the U(VI) and the adsorbents. As the U(VI) concentration continued to increase to 148.9 mg L^{-1}, the amount of U(VI) adsorbed by the PEM hardly changed since the limited adsorption sites on the adsorbents. At that time, the saturated adsorption capacity of PEM was calculated to be 485.9 mg g^{-1}. In order to obtain the sorption mode of U(VI) onto PEM, the experimental data were applied to Langmuir and Freundlich models. The Langmuir and the Freundlich models were used as the following formulas:

The Langmuir model equation: $\frac{C_e}{q_e} = \frac{1}{q_m K_L} + \frac{C_e}{q_m}$ (5)

The Freundlich model equation: $\mathrm{Ln}q_e = \mathrm{Ln}K_f + \frac{1}{n}\mathrm{Ln}C_e$ (6)

where q_e (mg g^{-1}) is the amount adsorbed at equilibrium, C_e (mg L^{-1}) is the equilibrium concentration, q_m (mg g^{-1}) is the maximum sorption capacity, and K_L (L mg^{-1}) is the Langmuir sorption equilibrium constant. K_f (mg g^{-1} (L mg^{-1})$^{1/n}$) is Freundlich constant which relates to the sorption capacity. n is the Freundlich constant to describe the sorption intensity. And the fitting plots as well as the parameters were given in Fig. S4 and Table S2. The Langmuir model showed a better R^2 value (0.995) and saturated capacity (505.05 mg g^{-1}) much closer to the experimental value (485.9 mg g^{-1}), indicating that the adsorption process of uranium onto PEM was the monolayer and uniform sorption mode. The comparison of uranium adsorption capacity and the optimal pH between PEM and some reported materials were listed in Table 2. It was noted that the PEM shows an excellent adsorption capacity of U(VI) under lower pH, which is possibly due to the good acid resistance of phosphate groups in PEM. All these mean that the PEM is promising in disposing of acidic uranium-containing wastewater.

Effect of temperature and thermodynamic studies

In order to evaluate the influence of temperature on adsorption and obtain the relevant thermodynamic parameters of the U(VI) sorption process, the adsorption experiments of U(VI) by PEM at different temperatures were conducted. Figure 8 showed that the adsorption capacity increased with the increase of temperature in the range of temperature 300–330 K, suggesting higher temperature was more beneficial to adsorption. Relevant data were fitted to get ΔH (KJ mol^{-1}), ΔS (J mol^{-1} k^{-1}) and G (KJ mol^{-1}) three thermodynamic parameters [31]:

$$K_d = \frac{q_e}{C_e} \quad (7)$$

$$\Delta G = \Delta H - T\Delta S \quad (8)$$

$$\mathrm{Ln}K_d = -\frac{\Delta H}{RT} + \frac{\Delta S}{R} \quad (9)$$

Table 2 The comparison between the PEM and other reported materials

Adsorbents	pH	q_m(mg g^{-1})	Refs.
Zn (HBTC)(L)	2.0	115	[40]
Wool-AO@TiO_2	8.0	113.12	[41]
HK@CMC	3.0	550	[42]
UiO-66-2COOH	4.0	150	[43]
COF-IHEP1	1.0	155	[24]
GPNB-BT	5.5	170	[44]
PAN-PEI/LDH	7.0	245.87	[45]
CCS	4.0	401.6	[46]
MA-U-PA	1.0	106.7	[47]
PM-9	4.0	1034.9	[31]
CA-PO_4	5.5	150.3	[48]
KIT-6-DAPhen	5.0	328	[49]
Fe_3O_4@nSiO_2@mSiO_2-DIM	5.5	100	[50]
PEM	4.0	505.05	This work

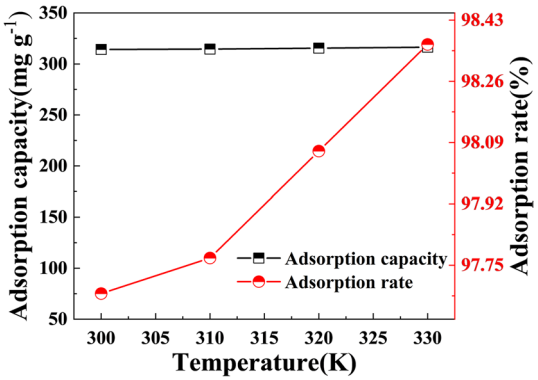

Fig. 8 The effect of T on the adsorption of U(VI) (C_0 = 160 mg L^{-1}, pH = 4.0, $m_{sorbent}/V_{solution}$ = 0.5 mg mL^{-1}, T = 298 K, Time = 60 min) and linearized plots of LnK_d versus T^{-1}

Table 3 Thermodynamic parameters for the adsorption

T (K)	ΔH (kJ mol^{-1})	ΔS (J mol^{-1} K^{-1})	ΔG (kJ mol^{-1})
300	9.996795	69.83511	− 10.9537
310			− 11.6521
320			− 12.3504
330			− 13.0488

where K_d (mL g^{-1}) is the distribution coefficient, R (0.008314 kJ mol^{-1} K^{-1}) is the gas constant, and T (K) is the absolute temperature. The linearized plots of LnK_d versus T^{-1} and the thermodynamic parameters were shown in Fig. S5 and Table 3 [49]. It was well known that the positive ΔH (99.67 kJ mol^{-1}) and negative ΔG indicated the endothermic and spontaneous properties of the adsorption process, respectively.

Adsorption mechanism

In Fig. 9, SEM images and EDS spectrum were adopted to observe the morphology and element changes of material after uranium adsorption (PEM-U). The distribution of U was clearly illustrated on the elemental mapping image of PEM-U. Additionally, the EDS spectrum of PEM-U showed that the atomic fraction of U was 22.41%, indicating the great adsorption performance of PEM.

To further investigate the functional groups involved in the uptake process, the FT-IR and Raman spectra of PEM before and after U(VI) sorption were collected and compared. As shown in Fig. 10a, an asymmetric peak of the UO_2^{2+} at 950 cm^{-1} occurred in the FT-IR spectrum of PEM-U [51], and the intensities of P=O and –NH_2 significantly weakened demonstrating the U(VI) were successfully adsorbed by PEM through interactions with P=O and –NH_2 [52]. Figure 10b presented the Raman spectrum of PEM and PEM-U. The characteristic Raman peak of UO_2^{2+} was found at 856 cm^{-1} [31, 51], whose result was corresponding with other measurements that the PEM had an effect on the adsorption of U(VI).

The XPS analysis was applied to determine the underlying sequestration mechanism. As shown in Fig. 11a, distinct peaks of U 4*f* were only observed after the uranium adsorption compared to the pristine PEM further indicating the favorable adsorption ability of the material [53]. There was no significant change in the C1*s*, which could be identified in Fig. 11c. In the O 1*s* spectra of PEM (Fig. 11d), the peaks at 532.15 eV, 531.24 eV, and 530.13 eV were attributed to O=P, O–P, and O–H, respectively. Peaks of O=P and O–H shifted to higher positions and their intensities in PEM-U were much lower than that in PEM revealing that U(VI) combined with the oxygen of the P=O and

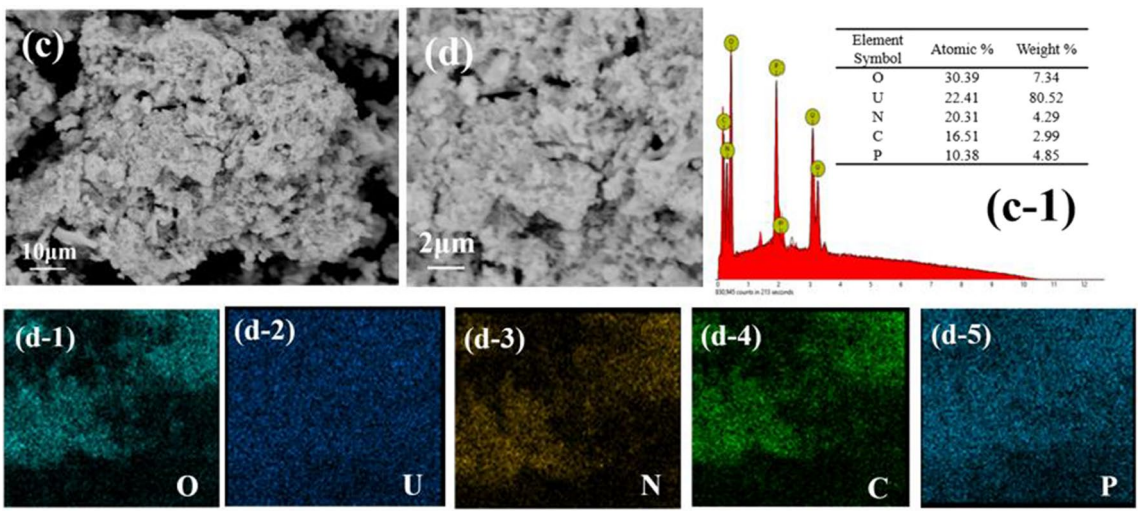

Fig. 9 SEM images and EDS spectrum of PEM-U

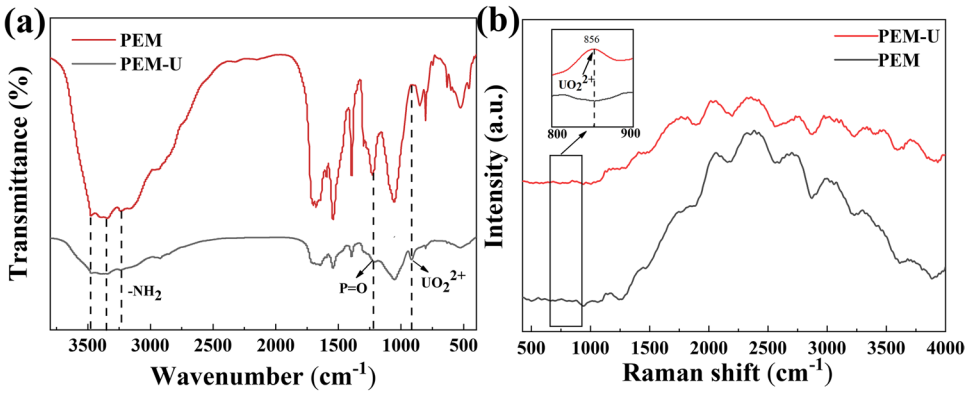

Fig. 10 **a** FT-IR spectra of PEM and PEM-U. **b** Raman spectra of PEM and PEM-U

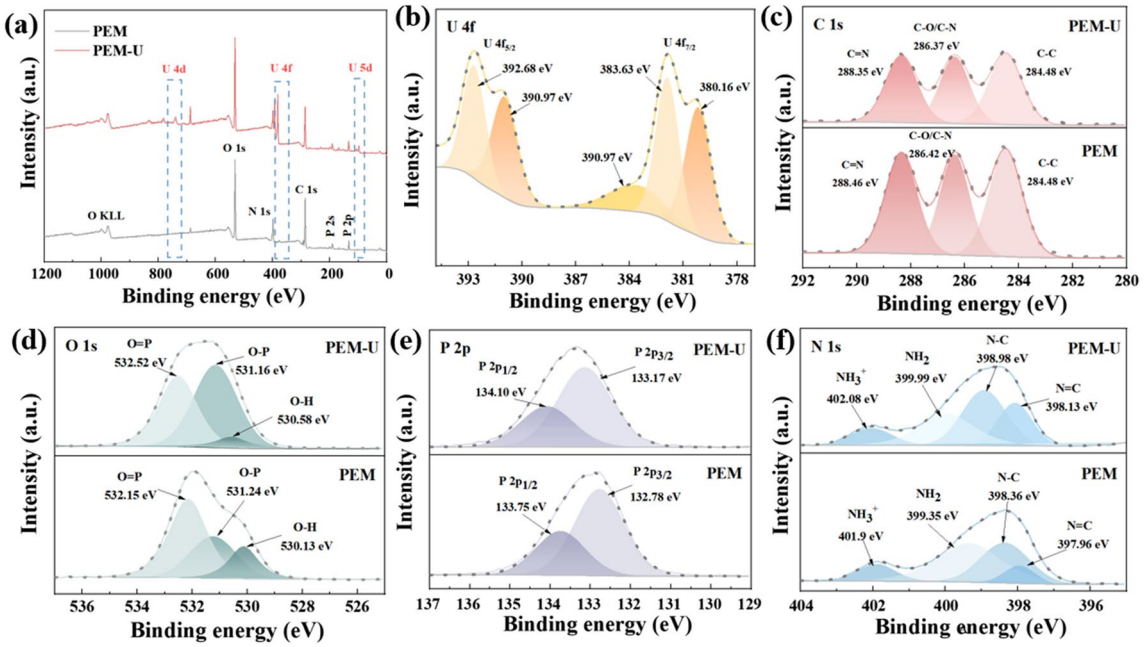

Fig. 11 **a** The typical XPS survey spectra of PEM and PEM-U. **b** High resolution XPS spectra for U4*f*, **c** C1*s*, **d** O1*s*, **e** P2*p*, **f** N1*s*

O–H group. In Fig. 11e, two close peaks in PEM located at 133.75 eV and 132.78 eV corresponded, respectively, to P 2*p*1/2 and P 2*p*3/2. The N1*s* core-level spectrum of PEM and PEM-U were shown in Fig. 11f [54]. According to Fig. 11e and f, the correlated peak areas in P 2*p* and N 1*s* varied, resulting from the chemical environment change before and after U(VI) attachment, indicating that P and N atoms of the related groups on PEM were involved in the complexation of U(VI). It was worth mentioning that the intensity of the NH_2 peak remarkably decreased from 46.04 to 28.47% following the U(VI) adsorption, which suggested the complexation of U(VI) with $–NH_2$ group of the PEM and in accordance with the analysis of FT-IR. The fine XPS spectra of uranium (Fig. 11b) elucidated that the adsorbed uranium was mainly in the hexavalent and tetravalent state, which meant, the redox immobilization of uranium was partially involved in the uranium adsorption process [55–57]

The uranium adsorption mechanism of PEM was deduced by the combination of SEM, FT-IR, Raman, XPS, adsorption isothermal, and adsorption kinetics analysis. The probable uranium adsorption mechanism was shown in Fig. 12. During the uranium capture, the equatorial plane perpendicular to the linear structure of U(VI) could chelate with the active groups, mainly $–NH_2$, P=O, and P–OH, in the presence of uranyl ion. The coordination ability of $P–O^-$ to cationic metal ions UO_2^{2+} originated predominantly from electrostatic forces since its negative charge, while the P=O group owning lone pairs of electrons could be donated into empty orbitals of U(VI). Numerous P–O and P=O onto the surface of PEM promoted U(VI) ion chelation to generate dentate ligands [58].

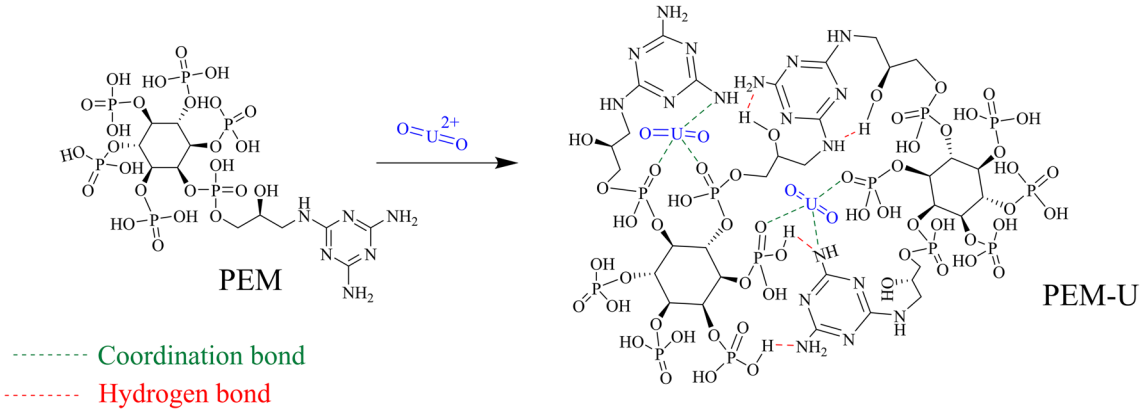

Fig. 12 Schematic representation of adsorption of U(VI) on PEM

Conclusion

A PA and MA covalent polymer (PEM) successfully prepared by the simple one-pot method was applied as an adsorbent for U(VI) enrichment and elimination. The amorphous PEM with rough, coral-like, and porous morphology could achieve efficient removal of U(VI) with a maximum uranium capacity of 505.05 mg g^{-1} at pH 4 derived from the Langmuir model, which was higher than most adsorbents under the same acidic condition. The adsorption reached equilibrium within 20 min at 298 K. Numerous active groups (mainly $–NH_2$, P=O, and P–OH) and the stable structure of the PEM were responsible for U(VI) adsorption by forming chelating species on the surface of the PEM. The adsorption process fitted well with the pseudo-second-order kinetics and Langmuir model, and the interaction between U(VI) and PEM was a spontaneous and endothermic process. The proposed strategy may also provide a practical, efficient, and optional for U(VI) capture in acidic nuclear fuel effluents.

Supplementary Information The online version contains supplementary material available at https://doi.org/10.1007/s10967-023-09100-2.

Acknowledgements This work was supported by the National Natural Science Foundation of China (22076155, 21976148, 11905177); Sichuan Science and Technology Program (2020JDRC0068); the Project of Science and Technology Department of Sichuan Province (No. 2021JDTD0019); the Project of State Key Laboratory of Environment-friendly Energy Materials, Southwest University of Science and Technology (Nos. 18fksy0215, 20fksy12); Undergraduate Innovation Fund Project of Southwest University of Science and Technology (CX22-016).

Author contributions Conceptualization: YW; Methodology: YW; Investigation: YW, SD, WS; Validation, formal analysis, and data curation: YW, SD, WS; Writing—original draft preparation: YW, SD, WS; Supervision, LZ; Project administration: TD, LZ; Funding acquisition: TD, LZ. All authors have read and agreed to the published version of the manuscript.

Data and code availability Data will be made available on request.

Declarations

Conflict of interest We declare that we do not have any commercial or associative interest that represents a conflict of interest in connection with the work submitted.

Ethical approval Ethical approval does not apply to this article.

References

1. He B, Yun Z, Shi J, Jiang G (2013) Research progress of heavy metal pollution in China: sources, analytical methods, status, and toxicity. Chin Sci Bull 58:134–140. https://doi.org/10.1007/s11434-012-5541-0
2. Shi S, Qian Y, Mei P, Yuan Y, Jia N, Dong M, Fan J, Guo Z, Wang N (2020) Robust flexible poly(amidoxime) porous network membranes for highly efficient uranium extraction from seawater. Nano Energy 71:104629. https://doi.org/10.1016/j.nanoen.2020.104629
3. Wang C-Z, Chai Z-F, Shi W-Q (2021) Ultrahigh affinity and selectivity nanotraps for uranium extraction from seawater. ACS Cent Sci 7:1602–1604. https://doi.org/10.1021/acscentsci.1c01118
4. Gavrilescu M, Pavel LV, Cretescu I (2009) Characterization and remediation of soils contaminated with uranium. J Hazard Mater 163:475–510. https://doi.org/10.1016/j.jhazmat.2008.07.103
5. Xie Y, Chen C, Ren X, Wang X, Wang H, Wang X (2019) Emerging natural and tailored materials for uranium-contaminated water treatment and environmental remediation. Prog Mater Sci 103:180–234. https://doi.org/10.1016/j.pmatsci.2019.01.005
6. Moraes MLB, Ladeira ACQ (2021) The role of iron in the rare earth elements and uranium scavenging by Fe–Al-precipitates in acid mine drainage. Chemosphere 277:130131. https://doi.org/10.1016/j.chemosphere.2021.130131
7. Shen J, Schafer A (2014) Removal of fluoride and uranium by nanofiltration and reverse osmosis: a review. Chemosphere 117:679–691. https://doi.org/10.1016/j.chemosphere.2014.09.090
8. Zhang Q, Larson SL, Ballard JH, Cheah P, Kazery JA, Knotek-Smith HM, Han FX (2020) A novel laboratory simulation system to uncover the mechanisms of uranium upward transport in a desert landscape. MethodsX 7:100758. https://doi.org/10.1016/j.mex.2019.11.031

9. Saito T, Sato K, Yamazawa H (2021) Numerical reproduction of dissolved U concentrations in a PO(4)-treated column study of Hanford 300 area sediment using a simple ion exchange and immobile domain model. J Environ Radioact 237:106708. https://doi.org/10.1016/j.jenvrad.2021.106708
10. Jun B-M, Lee H-K, Park S, Kim T-J (2021) Purification of uranium-contaminated radioactive water by adsorption: a review on adsorbent materials. Sep Purif Technol 278:119675. https://doi.org/10.1016/j.seppur.2021.119675
11. Kilinc E, Ozdemir S, Yalcin MS, Soylak M (2019) A magnetized fungal solid-phase extractor for the preconcentrations of uranium(VI) and thorium(IV) before their quantitation by ICP-OES. Mikrochim Acta 186:355. https://doi.org/10.1007/s00604-019-3474-x
12. Liu L, Liu J, Liu X, Dai C, Zhang Z, Song W, Chu Y (2019) Kinetic and equilibrium of U(VI) biosorption onto the resistant bacterium *Bacillus amyloliquefaciens*. J Environ Radioact 203:117–124. https://doi.org/10.1016/j.jenvrad.2019.03.008
13. Liu W, Dai X, Bai Z, Wang Y, Yang Z, Zhang L, Xu L, Chen L, Li Y, Gui D, Diwu J, Wang J, Zhou R, Chai Z, Wang S (2017) Highly sensitive and selective uranium detection in natural water systems using a luminescent mesoporous metal–organic framework equipped with abundant Lewis basic sites: a combined batch, X-ray absorption spectroscopy, and first principles simulation investigation. Environ Sci Technol 51:3911–3921. https://doi.org/10.1021/acs.est.6b06305
14. Ouchi K, Tsukahara T, Brandt A, Muto Y, Nabatame N, Kitatsuji Y (2021) Design of microchannel suitable for packing with anion exchange resins: uranium separation from seawater containing a large amount of cesium. Anal Sci 37:1789–1794. https://doi.org/10.2116/analsci.21P110
15. Niu CP, Zhang CR, Cui WR, Yi SM, Liang RP, Qiu JD (2022) A conveniently synthesized redox-active fluorescent covalent organic framework for selective detection and adsorption of uranium. J Hazard Mater 425:127951. https://doi.org/10.1016/j.jhazmat.2021.127951
16. Liu H, Fu T, Mao Y (2022) Metal–organic framework-based materials for adsorption and detection of uranium(VI) from aqueous solution. ACS Omega 7:14430–14456. https://doi.org/10.1021/acsomega.2c00597
17. Liao J, Liu P, Xie Y, Zhang Y (2021) Metal oxide aerogels: preparation and application for the uranium removal from aqueous solution. Sci Total Environ 768:144212. https://doi.org/10.1016/j.scitotenv.2020.144212
18. Chen Z, He X, Li Q, Yang H, Liu Y, Wu L, Liu Z, Hu B, Wang X (2022) Low-temperature plasma induced phosphate groups onto coffee residue-derived porous carbon for efficient U(VI) extraction. J Environ Sci (China) 122:1–13. https://doi.org/10.1016/j.jes.2021.10.003
19. Yang LX, Feng XF, Yin WH, Tao Y, Wu HQ, Li JQ, Ma LF, Luo F (2018) Metal–organic framework containing both azo and amide groups for effective U(VI) removal. J Solid State Chem 265:148–154. https://doi.org/10.1016/j.jssc.2018.05.040
20. Ismail AF, Yim M-S (2015) Investigation of activated carbon adsorbent electrode for electrosorption-based uranium extraction from seawater. Nucl Eng Technol 47:579–587. https://doi.org/10.1016/j.net.2015.02.002
21. Baybaş D, Ulusoy U (2011) The use of polyacrylamide-aluminosilicate composites for thorium adsorption. Appl Clay Sci 51:138–146. https://doi.org/10.1016/j.clay.2010.11.020
22. Tang N, Liang J, Niu C, Wang H, Luo Y, Xing W, Ye S, Liang C, Guo H, Guo J, Zhang Y, Zeng G (2020) Amidoxime-based materials for uranium recovery and removal. J Mater Chem A 8:7588–7625. https://doi.org/10.1039/C9TA14082D
23. Kabay N, Demircioğlu M, Yaylı S, Günay E, Yüksel M, Sağlam M, Streat M (1998) Recovery of uranium from phosphoric acid solutions using chelating ion-exchange resins. Ind Eng Chem Res 37:1983–1990. https://doi.org/10.1021/ie970518k
24. Yu J, Yuan L, Wang S, Lan J, Zheng L, Xu C, Chen J, Wang L, Huang Z, Tao W, Liu Z, Chai Z, Gibson John K, Shi W (2019) Phosphonate-decorated covalent organic frameworks for actinide extraction: a breakthrough under highly acidic conditions. CCS Chem 1:286–295. https://doi.org/10.31635/ccschem.019.20190005
25. Yu J, Lan J, Wang S, Zhang P, Liu K, Yuan L, Chai Z, Shi W (2021) Robust covalent organic frameworks with tailor-made chelating sites for synergistic capture of U(VI) ions from highly acidic radioactive waste. Dalton Trans 50:3792–3796. https://doi.org/10.1039/D1DT00186H
26. Budnyak TM, Gładysz-Płaska A, Strizhak AV, Sternik D, Komarov IV, Majdan M, Tertykh VA (2018) Imidazole-2yl-phosphonic acid derivative grafted onto mesoporous silica surface as a novel highly effective sorbent for uranium(VI) ion extraction. ACS Appl Mater Interfaces 10:6681–6693. https://doi.org/10.1021/acsami.7b17594
27. Jayakumar R, Selvamurugan N, Nair SV, Tokura S, Tamura H (2008) Preparative methods of phosphorylated chitin and chitosan—an overview. Int J Biol Macromol 43:221–225. https://doi.org/10.1016/j.ijbiomac.2008.07.004
28. Li H, Li Y, Zhou Y, Li B, Liu D, Liao H (2019) Efficient removal of uranium using a melamine/trimesic acid-modified hydrothermal carbon-based supramolecular organic framework. J Colloid Interface Sci 544:14–24. https://doi.org/10.1016/j.jcis.2019.02.079
29. Wang X, Li R, Liu J, Chen R, Zhang H, Liu Q, Li Z, Wang J (2017) Melamine modified graphene hydrogels for the removal of uranium(VI) from aqueous solution. New J Chem 41:10899–10907. https://doi.org/10.1039/C7NJ01927K
30. Huang J, Liu Z, Huang D, Jin T, Qian Y (2022) Efficient removal of uranium (VI) with a phytic acid-doped polypyrrole/carbon felt electrode using double potential step technique. J Hazard Mater 433:128775. https://doi.org/10.1016/j.jhazmat.2022.128775
31. Pan N, Jin Y, Wang X, Hu X, Chi F, Zou H, Xia C (2019) A self-assembled supramolecular material containing phosphoric acid for ultrafast and efficient capture of uranium from acidic solutions. ACS Sustain Chem Eng 7:950–960. https://doi.org/10.1021/acssuschemeng.8b04596
32. Li G, Shang Y, Wang Y, Wang L, Chao Y, Qi Y (2019) Reaction mechanism of etherification of rice straw with epichlorohydrin in alkaline medium. Sci Rep 9:14307. https://doi.org/10.1038/s41598-019-50860-3
33. Dave G, Modi H (2018) FT-IR method for estimation of phytic acid content during bread-making process. J Food Meas Charact 12:2202–2208. https://doi.org/10.1007/s11694-018-9836-y
34. Pande R, Mishra HN (2015) Fourier transform near-infrared spectroscopy for rapid and simple determination of phytic acid content in green gram seeds (*Vigna radiata*). Food Chem 172:880–884. https://doi.org/10.1016/j.foodchem.2014.09.049
35. Yang S, Zhang B, Liu M, Yang Y, Liu X, Chen D, Wang B, Tang G, Liu X (2021) Fire performance of piperazine phytate modified rigid polyurethane foam composites. Polym Adv Technol 32:4531–4546. https://doi.org/10.1002/pat.5454
36. Idris SA, Davidson CM, McManamon C, Morris MA, Anderson P, Gibson LT (2011) Large pore diameter MCM-41 and its application for lead removal from aqueous media. J Hazard Mater 185:898–904. https://doi.org/10.1016/j.jhazmat.2010.09.105
37. Zhang J-Y, Zhang N, Zhang L, Fang Y, Deng W, Yu M, Wang Z, Li L, Liu X, Li J (2015) Adsorption of uranyl ions on amine-functionalization of MIL-101(Cr) nanoparticles by a facile

coordination-based post-synthetic strategy and X-ray absorption spectroscopy studies. Sci Rep 5:13514. https://doi.org/10.1038/srep13514
38. Xiong T, Li Q, Liao J, Zhang Y, Zhu W (2022) Highly enhanced adsorption performance to uranium(VI) by facile synthesized hydroxyapatite aerogel. J Hazard Mater 423:127184. https://doi.org/10.1016/j.jhazmat.2021.127184
39. Liu J, Zhao C, Zhang Z, Liao J, Liu Y, Cao X, Yang J, Yang Y, Liu N (2016) Fluorine effects on U(VI) sorption by hydroxyapatite. Chem Eng J 288:505–515. https://doi.org/10.1016/j.cej.2015.12.045
40. Wang LL, Luo F, Dang LL, Li JQ, Wu XL, Liu SJ, Luo MB (2015) Correction: ultrafast high-performance extraction of uranium from seawater without pretreatment using an acylamide- and carboxyl-functionalized metal–organic framework. J Mater Chem A 3:17880–17880. https://doi.org/10.1039/C5TA90169C
41. Wen J, Li Q, Li H, Chen M, Hu S, Cheng H (2018) Nano-TiO_2 imparts amidoximated wool fibers with good antibacterial activity and adsorption capacity for uranium(VI) recovery. Ind Eng Chem Res 57:1826–1833. https://doi.org/10.1021/acs.iecr.7b04380
42. Zeng D, Yuan L, Zhang P, Wang L, Li Z, Wang Y, Liu Y, Shi W (2021) Hydrolytically stable foamed HKUST-1@CMC composites realize high-efficient separation of U(VI). iScience 24:102982. https://doi.org/10.1016/j.isci.2021.102982
43. Zhao B, Yuan L, Wang Y, Duan T, Shi W (2021) Carboxylated UiO-66 tailored for U(VI) and Eu(III) trapping: from batch adsorption to dynamic column separation. ACS Appl Mater Interfaces 13:16300–16308. https://doi.org/10.1021/acsami.1c00364
44. Meng J, Lin X, Zhou J, Zhang R, Chen Y, Long X, Shang R, Luo X (2019) Preparation of tannin-immobilized gelatin/PVA nanofiber band for extraction of uranium(VI) from simulated seawater. Ecotoxicol Environ Saf 170:9–17. https://doi.org/10.1016/j.ecoenv.2018.11.089
45. Li W, Chen R, Liu Q, Liu J, Yu J, Zhang H, Li R, Zhang M, Wang J (2018) Hierarchical Ni–Al layered double hydroxide in situ anchored onto polyethylenimine-functionalized fibers for efficient U(VI) capture. ACS Sustain Chem Eng 6:13385–13394. https://doi.org/10.1021/acssuschemeng.8b03183
46. Li L, Huang S, Wen T, Ma R, Yin L, Li J, Chen Z, Hayat T, Hu B, Wang X (2019) Fabrication of carboxyl and amino functionalized carbonaceous microspheres and their enhanced adsorption behaviors of U(VI). J Colloid Interface Sci 543:225–236. https://doi.org/10.1016/j.jcis.2019.02.060
47. Liang L, Zhang H, Lin X, Yan K, Li M, Pan X, Hu Y, Chen Y, Luo X, Shang R (2021) Phytic acid-decorated porous organic polymer for uranium extraction under highly acidic conditions. Colloids Surf A. https://doi.org/10.1016/j.colsurfa.2021.126981
48. Zhang Z, Dong Z, Wang X, Dai Y, Cao X, Wang Y, Hua R, Feng H, Chen J, Liu Y, Hu B, Wang X (2019) Synthesis of ultralight phosphorylated carbon aerogel for efficient removal of U(VI): batch and fixed-bed column studies. Chem Eng J 370:1376–1387. https://doi.org/10.1016/j.cej.2019.04.012
49. Yuan L-Y, Zhu L, Xiao C-L, Wu Q-Y, Zhang N, Yu J-P, Chai Z-F, Shi W-Q (2017) Large-pore 3D cubic mesoporous (KIT-6) hybrid bearing a hard-soft donor combined ligand for enhancing U(VI) capture: an experimental and theoretical investigation. ACS Appl Mater Interfaces 9:3774–3784. https://doi.org/10.1021/acsami.6b15642
50. Zhu L, Yuan L-Y, Xia L-S, Wang L (2016) Incorporation of magnetism into the dihydroimidazole functionalized mesoporous silica for convenient U(VI) capture. J Radioanal Nucl Chem 308:447–458. https://doi.org/10.1007/s10967-015-4391-z
51. Bagnall KW, Wakerley MW (1975) Infrared and Raman spectra of the uranyl ion. J Inorg Nucl Chem 37:329–330. https://doi.org/10.1016/0022-1902(75)80194-1
52. Huynh J, Palacio R, Safizadeh F, Lefevre G, Descostes M, Eloy L, Guignard N, Rousseau J, Royer S, Tertre E, Batonneau-Gener I (2017) Adsorption of uranium over NH_2-functionalized ordered silica in aqueous solutions. ACS Appl Mater Interfaces 9:15672–15684. https://doi.org/10.1021/acsami.6b16158
53. Tovar-Valdín G, Ordóñez-Regil E, Almazán-Torres M-G, Martínez-Gallegos S (2018) Synthesis and characterization of phytate–uranium(VI) complexes. J Radioanal Nucl Chem 318:2129–2137. https://doi.org/10.1007/s10967-018-6296-0
54. Stevens JS, Byard SJ, Seaton CC, Sadiq G, Davey RJ, Schroeder SLM (2014) Proton transfer and hydrogen bonding in the organic solid state: a combined XRD/XPS/ssNMR study of 17 organic acid–base complexes. Phys Chem Chem Phys 16:1150–1160. https://doi.org/10.1039/C3CP53907E
55. Qiang S, Wang J, Wang Y, Yuan L, Shi L, Ding Z, Wang W, Liang J, Li P, Fan Q (2022) Analysis of the uranium chemical state by XPS: Is what you see real? Appl Surf Sci 576:151886. https://doi.org/10.1016/j.apsusc.2021.151886
56. Ding L, Chen B, Wang Y, Zhang Y (2022) High efficiency adsorption of uranium in solution using nano-TiO_2 loaded with g-C_3N_4. Process Saf Environ Prot 168:1049–1057. https://doi.org/10.1016/j.psep.2022.10.055
57. Xiong T, Jia L, Li Q, Zhang Y, Zhu W (2022) Highly efficient adsorptive extraction of uranium from wastewater by novel kaolin aerogel. Sci Total Environ 842:156916. https://doi.org/10.1016/j.scitotenv.2022.156916
58. Zheng T, Wu Q-Y, Gao Y, Gui D, Qiu S, Chen L, Sheng D, Diwu J, Shi W-Q, Chai Z, Albrecht-Schmitt TE, Wang S (2015) Probing the influence of phosphonate bonding modes to uranium(VI) on structural topology and stability: a complementary experimental and computational investigation. Inorg Chem 54:3864–3874. https://doi.org/10.1021/acs.inorgchem.5b00024

Publisher's Note Springer Nature remains neutral with regard to jurisdictional claims in published maps and institutional affiliations.

Springer Nature or its licensor (e.g. a society or other partner) holds exclusive rights to this article under a publishing agreement with the author(s) or other rightsholder(s); author self-archiving of the accepted manuscript version of this article is solely governed by the terms of such publishing agreement and applicable law.